International Journal of Nanomedicine

Dovepress
open access to scientific and medical research

Open Access Full Text Article

ORIGINAL RESEARCH

Microspheres of alginate encapsulated minocycline-loaded nanocrystalline carbonated hydroxyapatite: therapeutic potential and effects on bone regeneration

This article was published in the following Dove Press journal:
International Journal of Nanomedicine

Mônica Diuana Calasans-Maia[1]
Carlos Alberto Brazil Barboza Junior[2]
Carlos Alberto Soriano-Souza[3]
Adriana Terezinha Neves Novellino Alves[4]
Marcelo Jose de Pinheiro Uzeda[1]
Victor R Martinez-Zelaya[3]
Elena Mavropoulos[3]
Maria Helena Rocha Leão[5]
Ronaldo Barcellos de Santana[2]
Jose Mauro Granjeiro[1]
Alexandre Malta Rossi[3]

[1]Clinical Research in Dentistry Laboratory, School of Dentistry, Federal Fluminense University, Niterói, Rio de Janeiro, Brazil; [2]Department of Periodontology, School of Dentistry, Federal Fluminense University, Niterói, Rio de Janeiro, Brazil; [3]Department of Condensed Matter, Applied Physics and Nanoscience, Brazilian Center for Research in Physics, Rio de Janeiro, Brazil; [4]Department of Stomatology. School of Dentistry, Federal Fluminense University, Niterói, Rio de Janeiro, Brazil; [5]Department of Biochemical Engineering, School of Chemistry, Federal University of Rio de Janeiro, Rio de Janeiro, Brazil

Correspondence: Mônica Diuana Calasans-Maia
Clinical Research in Dentistry Laboratory, School of Dentistry, Federal Fluminense University, Niterói, Rio de Janeiro 24.020-150, Brazil
Email monicacalasansmaia@gmail.com

Background and objective: Tetracycline and its derivatives, combined with calcium phosphates, have been proposed as a delivery system to control inflammatory processes and chronic infections. The objective of this study was to evaluate the microspheres of alginate encapsulated minocycline-loaded nanocrystalline carbonated hydroxyapatite (CHAMINO) as a biomimetic device to carry out target-controlled drug delivery for alveolar bone repair.

Methods: CHAMINO microspheres were implanted in a rat central incisor socket after 7 and 42 days. New bone was formed in both groups between 7 and 42 days of implantation. However, the bone growth was significantly higher for the CHAMINO microspheres.

Results: The minocycline (MINO) loading capacity of the nanocrystaline carbonated hydroxyapatite (CHA) nanoparticles was 25.1±2.2 µg MINO/mg CHA for adsorption over 24 hrs. The alginate microspheres containing minocycline-loaded CHA were biologically active and inhibited the *Enterococcus faecalis* culture growth for up to seven days of the MINO release. An osteoblastic cell viability assay based on the resazurin reduction was conducted after the cells were exposed to the CHAMINO powder and CHAMINO microspheres. Thus, it was found that the alginate extracts encapsulated the minocycline-loaded CHA microspheres and did not affect the osteoblastic cell viability, while the minocycline-doped CHA powder reduced the cell viability by 90%.

Conclusion: This study concluded that the alginate microspheres encapsulating the minocycline-loaded nanocrystalline carbonated hydroxyapatite exhibited combined antibacterial activity against *Enterococcus faecalis* with cytocompatibility and osteoconduction properties. The significant improvement in the new bone formation after 42 days of implantation suggests that the CHAMINO microsphere has potential in clinical applications of bone regeneration.

Keywords: nanomaterials, carbonated hydroxyapatite, minocycline, biocompatibility, bone regeneration

Introduction

Hydroxyapatite (HA) is one of the most important bioactive ceramics used in medicine and dentistry, owing to its biocompatibility and osteoconduction properties.[1,2] The controlled delivery of therapeutic substances by hydroxyapatite has been proposed as a viable approach to prevent and control inflammatory processes, chronic infections, and to enhance the endogenous healing capacity of

bone defects, which ultimately result in the significant improvement of bone regeneration.[3,4,5] The main limitation of HA ceramics is their high crystallinity, low adsorption capacity for drugs, and poor *in-vivo* bioabsorbability. Nanocrystaline hydroxyapatite (nHA) is an alternative to HA ceramics as a drug delivery carrier, owing to its high and reactive surface area, nanoscale porosity, and in vivo degradability.[6] Several strategies have been developed to associate nHA with a large number of antibiotics, particularly tetracyclines,[7,8] gentamicin,[9,10] and vancomycin.[11,12] The efficiency of the delivery system depends on the interaction of antibiotics with the nHA surface, scaffold porosity, antibiotic loading capacity on the nHA nanoparticles, and sustained release in the diseased defect.[13] Apart from its therapeutic activity, nHA also acts as a bioactive matrix for newly formed bone, which may be improved with metal (Zn^{2+} and Sr^{2+}) and carbonate substitution (CO_3^{2-}) in the apatite structure.[14–16]

Tetracyclines and its derivatives such as doxycycline, minocycline, and tigecycline associated with nHA have been proposed for the treatment of bone and oral infections, including marginal periodontitis, infected root canals, and periradicular abscesses.[17–20] The loading capacities of tetracyclines are sensitive to the microstructure and nanostructure of nHA[21] and to the composition of the delivery vehicle. Previous in vitro studies have shown that the release of tetracyclines can be sustained for more than five days using i) calcium phosphate foams,[22] ii) nHA microspheres with polycaprolactone (PCL), poly(lactic-co-glycolic acid) (PLGA),[23,24] iii) biphasic calcium phosphate encapsulated in PCL, PLGA, and β-cyclodextrin (βCD),[25] and iv) nHA associated with gelatine fibrils.[26] Despite efforts to develop efficient delivery nHA devices, few studies have been conducted on the in vivo behavior of tetracycline-loaded nHA systems with regard to bone formation. Recently, Ding et al implanted a titanium screw coated with doxycycline-loaded HA in mice teeth and observed higher bone formation around the implant for the doxycycline-coated implants.[27] According to the authors, the improvement of bone formation was related to the inhibitory effect of doxycycline on the inflammatory response.

In this study, alginate encapsulated nanocrystalline carbonated hydroxyapatite (CHA) microspheres were evaluated as a biomimetic device for the local delivery of minocycline to inhibit the growth of *Enterococcus faecalis*. Moreover, we investigated the in vitro cytocompatibility and in vivo biocompatibility of the minocycline-loaded microspheres, and the effect of minocycline delivery on new bone formation.

Materials and Methods

Carbonated hydroxyapatite preparation

Nanocrystalline carbonated hydroxyapatite (CHA) powder was prepared by the drop-wise addition of aqueous extra-pure calcium nitrate tetrahydrate [$Ca(NO_3)_2.4H_2O$] (Merck®), dihydrogen ammonium phosphate [$(NH_4)2HPO_4$] (Merck®), and ammonium carbonate [$(NH_4)2CO_3$] (Merck®). The reagents were mixed and maintained at 37°C for 2 hrs at pH 9 in the presence of KOH (Merck®). The calcium and phosphorous concentrations were determined from the wavelength-dispersive X-ray fluorescence (WDXRF) using a PW 2400 Sequential Wavelength X-Ray Spectrometer (Philips Analytical X-Ray, Almelo, Netherlands) at 3.0 KV. The samples were prepared by fusion with lithium tetraborate ($Li_2B_4O_7$).

Minocycline adsorption onto carbonated hydroxyapatite

The adsorption of minocycline (MINO) onto the CHA was performed according to the procedure described by Soriano-Souza et al[28] Briefly, CHA was incubated in 0.15% minocycline hydrochloride (Sigma-Aldrich) phosphate-buffered saline (PBS, pH 7.4) solutions at a proportion of 50 mg CHA/mL MINO for 24 hrs. After incubation in the MINO solutions, the powder was centrifuged at 6,000 RPM for 5 mins, slightly washed for 1 min to remove the physically adsorbed MINO fractions, dried using the freeze-lyophilization method for 24 hrs and sterilized by gamma-rays (15 kGy). The concentration of the MINO adsorbed onto the CHA surface was determined using UV-Vis spectrophotometry at a wavelength of 245 nm (UV-Vis 2550 Spectrophotometer, Shimadzu Corp.)

Preparation of carbonated hydroxyapatite microspheres

CHA powders with or without MINO were gently dispersed in a 10 mg/mL aqueous solution of sodium alginate (Fluka Biochemika, Buchs, Switzerland) to achieve a 1:15 alginate-CHA ratio. The alginate/CHA mixture was extruded drop-wise into a 0.35 M $CaCl_2$ solution at room temperature using a needle with a diameter of 0.70 mm (BD Precision Glide, Sao Paulo, SP, Brazil). Spherical particles instantaneously formed and were allowed to mature in the $CaCl_2$ solution for 15 mins, for gelation to

occur. The CHA-alginate microspheres were dried using the freeze-lyophilization method for 24 hrs and sterilized by gamma rays (15 kGy). Additionally, the microspheres were characterized by X-ray diffraction (X'Pert Pro X-Ray diffractometer) and Fourier transform infrared spectroscopy (IR Prestige Series 21), respectively. The specific surface area of the microspheres was determined by the BET method using the ASAP 2020 instrument (Micromeritics Instrument Corp., Norcross, USA). The morphology of the implants was investigated using scanning electron microscopy (SEM; JEOL JSM 5310).

Physico-chemical characterization of experimental biomaterials

The structure and crystallinity of CHA were analyzed using a Fourier transform infrared spectrophotometer (FTIR) (IRPrestige-21, Shimadzu, CBPF-RJ) in transmission mode from 400 to 4,000 cm^{-1}, and X-ray diffraction (XRD) (X'Pert Pro X-Ray diffractometer, PANanalytical) operating with CuKα radiation (1.5418 Å) at 40 kV and 40 mA. The XRD data were compared with the standards of file 9–432 from the International Centre for Diffraction Data (ICDD) using the PCPDF Win 2.1 software. The Brunauer, Emmett, and Teller Method (BET) was used to determine the CHA microsphere surface area and nanoporosity using an ASAP 2020 Accelerated Surface Area and Porosimetry Analyzer (Micromeritcs, USA). Synchrotron radiation-based X ray microtomography (SR-μCT) was used to characterize the internal structure of the CHA microsphere. The samples were analyzed with a micro X-ray scanned at the high-resolution imaging beamline (IMX) at the Brazilian Synchrotron Light Source (LNLS). The samples were illuminated by a polychromatic beam (4–24 keV) and a 550 μm Si filter was positioned before the sample to reduce the beam hardening effect.[29] Moreover, 1,001 projections were captured using a CCD camera (PCO.2000), and a 10X lens was used to magnify the image and obtain a pixel size of 0.82 μm. The experiments were performed in contrast mode and the count mode was used to guarantee the same flux on all projections, because the beam current had a half-time of 12 hrs and changed considerably during the experiment (typically, one full three-dimensional (3D) scan takes 45 mins). A fast backprojection algorithm was used to reconstruct the data, whereas Avizo 9.5,[30,31] which is a 3-D visualization software, was used to filter, segment, and analyze the images and determine the internal pore distribution and equivalent pore diameter.

Minocycline in vitro release assays

MINO release assays were carried out in vitro by incubating the alginate encapsulated minocycline-loaded nanocrystalline carbonated hydroxyapatie (CHAMINO) microsphere samples in PBS for up to 10 days. Briefly, 100 mg of CHAMINO microspheres were incubated in 10 mL of pH 7.4 PBS at 37°C. The supernatant was collected at defined intervals of 1 to 60 mins at 1, 3, 5, 7, and 10 days. A new aliquot of PBS was added for each day interval up to 10 days when the final sample was collected. Then, the amount of the released MINO was determined using UV-Vis spectrophotometry at 245 nm (UV-Vis 2550 Spectrophotometer, Shimadzu Corp.).

Microbiological assays

The antimicrobial activity tests were based on standard dilution methods published by the National Committee for Clinical Laboratory Standards.[32] Briefly, *E. faecalis* (ATCC 29212), which are able to survive various stresses and hostile environments, were grown from frozen stocks in trypticase soy broth (TSB; Plast Labor, Rio de Janeiro, RJ, Brazil). The cultures were freshly prepared for each experiment and diluted to 0.5 of the McFarland turbidity standards, to approximately 1.5×10^8 cells/mL. The bacteria were incubated in TSB containing CHAMINO microspheres (25 mg CHAMINO/mL to 0.012 mg CHAMINO/mL concentrations), at 1, 3, 5, and 7 days before and after the released tests. The minimum inhibitory concentrations (MIC) were determined using standard dilution methods (1:1 to 1:2,048). To evaluate the ability of growth inhibition, after 18 hrs, the broth turbidity was measured using a UV spectrophotometer at 595 nm (UV-VIS 2550, Shimadzu, Japan). The MIC values were defined by the lowest dilution to keep the culture medium free of turbidity. All tests were conducted in triplicate.

Cell culture experiments

Osteoblast cells from the periosteum-free fragments of murine femurs (F-OST) were used in this study.[33] The cells were cultured in Dulbecco's modified essential medium (DMEM, Gibco) supplemented with 10% fetal bovine serum (FBS) at 37°C and 5% CO_2. Semi-confluent cells were trypsinized, counted in a Neubauer chamber, and used in all experiments. Control samples were cultured in 13-mm Thermanox coverslips (Thermo Scientific Nunc

Inc., Rochester, USA) pre-coated with 0.1% porcine gelatin.

Cytocompatibility assay

A cell viability assay based on the ISO 10993–5:2009 protocol was conducted after exposing the F-OST osteoblastic cell to the extract of each material (CHA powder, CHA microspheres, CHAMINO powder, and CHAMINO microspheres) to determine whether the alterations in the cell behavior were associated with the release of MINO.[34] The conditioned media extracts were prepared by mixing 100 mg of each material with 1 mL of DMEM medium under slow agitation at 37°C for 24 hrs. The cells were seeded into 96-well culture plates with a density of 8×10^3 cells/well, and incubated in the presence of the extracts for 24 hrs at 37°C under 5% CO_2. The cells cultured in the DMEM medium supplemented with FBS were used as a negative control (C-), and a 1% sodium dodecyl sulfate (SDS) and MINO 0.25% solution was used as the positive control (C+; MINO). At the end of the incubation period, the cells were washed with PBS, and viability tests were carried out. After sample exposure, the cell viability was determined using PrestoBlue® (PB) reagent (InvitroGen, USA). The reagent is a solution based on resazurin (7-hydroxy-3H-phenoxazine-3-one-10-oxide), and the viable cells reduce this compound to resafurin through a process accompanied by the color and fluorescence changes detected in the solution at 590 nm. Briefly, after incubation, 10 µL of reagent PB was added to each well of a 96-well plate containing 90 µL of media and osteoblastic cells. The plate was incubated for 10 min at 37°C and 5% CO_2 under a humidified atmosphere. Then, the cell viability was determined by measuring the resulting fluorescent signal.

In Vivo biocompatibility assays

Animals and surgical procedures

All procedures were carried out in accordance with the conventional guidelines in the Guide for the Care and Use of Laboratory Animals (US National Institutes of Health 85–23, revised 1996) and were approved by the local Institutional Animal Care and Use Committee of the Federal Fluminense University, Niteroi, Brazil (protocol number 50). This study is reported according to the ARRIVE guidelines (Animal Research: Reporting of In Vivo Experiments) with regard to the relevant items.[35] Three-month-old male Wistar rats weighing approximately 250 g were kept under standard conditions with free access to food and water. A total of 20 animals were divided into 2 groups and investigated after 2 experimental periods (7 and 42 days). All animals were anesthetized with ketamine (20 mg/kg) (Virbac, Jurubatuba, SP, Brazil) and xylazine (1 mg/Kg) (FortDodge, São Cristovão, RJ, Brazil). The surgical area was scrubbed with a sterile gauze soaked with 1.2% chlorhexidine, rinsed with sterile water, and then draped. Subsequently, the syndesmotomy of the periodontal tissue was performed using a syndesmotome (Duflex®, Rio de Janeiro, Rio de Janeiro, Brazil), and the upper-right incisor was extracted with a clinical probe adapted to this tooth. The dental alveolar sockets were grafted either with nanocrystalline carbonated hydroxyapatite microspheres (CHA group, n=10) or with CHA incorporated with MINO (CHAMINO, n=10), and sutured with a 5–0 nylon interrupted suture. (Johnson & Johnson Medical Ltd., Blue Ash, Ohio, United States). At 7 and 42 days after implantation, the animals were euthanized with an overdose of the anesthetic solution and the samples containing the biomaterials were removed and fixed in 4% buffered formalin at pH 7.0. The specimens were decalcified in a fast bone demineralization solution (Allkimia Ltda., Campinas, Brazil) for 48 hrs, washed for 1 hr, dehydrated in ethanol (Vetec Química Fina Ltda., Duque de Caxias, Brazil), clarified in xylol (Vetec Ltda.), and embedded in paraffin (Vetec Ltda.).

Histological and histomorphometric analysis

Decalcified paraffin sections (thickness of 5 µm) were stained with hematoxylin-eosin (HE) and investigated by a pathologist who was experienced in the field of biomaterial biocompatibility but did not have knowledge of the tested animal groups (blind analysis). A descriptive analysis comparing the intra- and intergroup biological responses was based on the type and intensity of the inflammatory alterations and repair processes (fibrosis, new blood vessels, and osteogenesis). Photomicrographs were obtained through a computer software (Olympus CellSens Platform) communicating with an optical microscope (Olympus BX 43, Tokyo, Kanto, Japan).

For histomorphometric analysis, a light microscope (Olympus BX 43, Tokyo, Kanto, Japan) with 10X magnification was used. The microscope was connected to a computer and each HE-stained histological slice corresponding to the alveolar region was captured through scanning and an image acquisition software (Cellsens® 1.9 Digital, Tokyo, Kanto, Japan). One expert observer analyzed ten non-consecutive images from each section. Using the Image-Pro Plus® 6.0 software (Media

Cybernetics, Silver Spring, Maryland, USA), a grid of 200 points was superimposed onto the captured field, which allowed us to determine the newly formed bone and residual biomaterial. The bone volume density (BV/TV%) was calculated by the bone volume over the total volume, which indicates the fraction of the volume of interest that was occupied by bone. The same method was applied to calculate the biomaterial volume density (BiomatV/TV%) and the volume density of the connective tissue (CT/TV%). The calculated areas were expressed as a percentage.

Statistical analysis

After the normality test, histological and histomorphometric analysis, a quantitative description, including the mean and confidence interval (CI) of BV/TV% and BiomatV/TV%, was performed. Analysis of variance was conducted using two-way ANOVA and Tukey's post-hoc test. Additionally, the two assignable sources of variation, groups, and periods, were evaluated. The significance level was set to p=0.05. The analyses were performed using the Prism Graph Pad® 6.3 software (GraphPad Software Inc., La Jolla, California, USA). For the cytocompatibility evaluation, the mean values and standard deviation for each test were calculated, and ANOVA with Dunnett's test was performed. The significance level was set to 99.9% (p<0.001).

Results

The CHA powder exhibited an XRD pattern typical of the nanocrystalline hydroxyapatite phase, as shown in Figure 1A. The Fourier transformed infrared (FTIR) spectrum confirmed the formation of carbonated doped hydroxyapatite, as shown in Figure 1B. The apatite phosphate bands were observed at 1,092 cm^{-1} (ν_3), 1,039 (ν_3), cm^{-1}, 957 cm^{-1}, (ν_1), 602 cm^{-1} (ν_4), and 563 cm-1 (ν_4), while the bands at 1,419 cm^{-1} and 1,458 cm^{-1} were assigned to carbonate groups occupying the phosphate sites in the apatite structure. The calcium for the phosphate ratio (Ca/P=2.070), which was determined by chemical analysis, reinforced the PO_4^{3-} for CO_3^{2-} substitution. The results obtained by BET analysis revealed that the CHA powder was composed of small aggregates consisting of CHA nanoparticles with a mean pore size of 2 nm to 94 nm and a specific surface area of 95 m^2/g, as presented in Table 1. The morphology of the CHA and CHAMINO microspheres was investigated using scanning electron microscopy, and it was revealed that the surfaces had different surface porosities, as shown in Figure 2.

The microspheres consisted of CHA nanoparticle (NP) agglomerates embedded in the biopolymer matrix. The gelling process and drying generated an irregular microroughness on the sphere surface, as shown in the SR-μCT image in Figure 3A. Additionally, SR-μCT analysis revealed that the internal sphere volume was occupied by CHA NP aggregates (63%) and interconnected micropores filled with alginate (23%), as shown in Figure 3B-D. The micropores had irregular morphology with an equivalent diameter of 14.8 μm (Figures 3 and S1).

Minocycline release assays and microbiological assays

The amount of MINO adsorbed on the CHA powder depended on the MINO initial concentration in the solution, the CHA mass, and the solution pH. The adsorption experiments were conducted with 1.5 mg/mL MINO in a PBS buffer solution (pH=7.4) containing 50 mg/mL of CHA powder. After incubation for 24 hrs, the amount of the antibiotic loaded onto the CHA powder was 25.1±2.2 μgMINO/mgCHA. The loss of MINO in the CHA power during the microsphere processing was approximately 40%. Figure 4 shows the MINO release profile from the CHA microspheres loaded with 15.1±1.4 μgMINO/mgCHA, in the PBS buffer. The fast release of approximately 60% of the initial loaded MINO (9.1 μgMINO/mgCHA) was observed during the first 24 hrs. The remaining 6.0 μg MINO/mgCHA was continuously released during a period of 10 days, as shown in Figure 4.

Microbiological assays were performed to evaluate the effects of minocycline-loaded CHA microspheres on the growth of *E. faecalis*. The minimum inhibitory concentration (MIC) was estimated using a standard dilution method from 25 mg of CHA microspheres loaded with 15 μg MINO per mg of CHA incubating in 1 mL of *E. faecalis* culture. As shown in Figure 4, the bacterial growth was inhibited with 0.2 mg of minocycline-doped CHA microspheres. This corresponded to the antibacterial effect (MIC) exerted by 3 μg of MINO in 1 mL of *E. faecalis* culture. A similar MIC assay was performed using minocycline-loaded microspheres after incubation in the PBS for 1, 3, 5, and 7 days. The results presented in Figure 4 reveal that the CHA microspheres were biologically active for the samples subjected to desorption for up to 7 days.

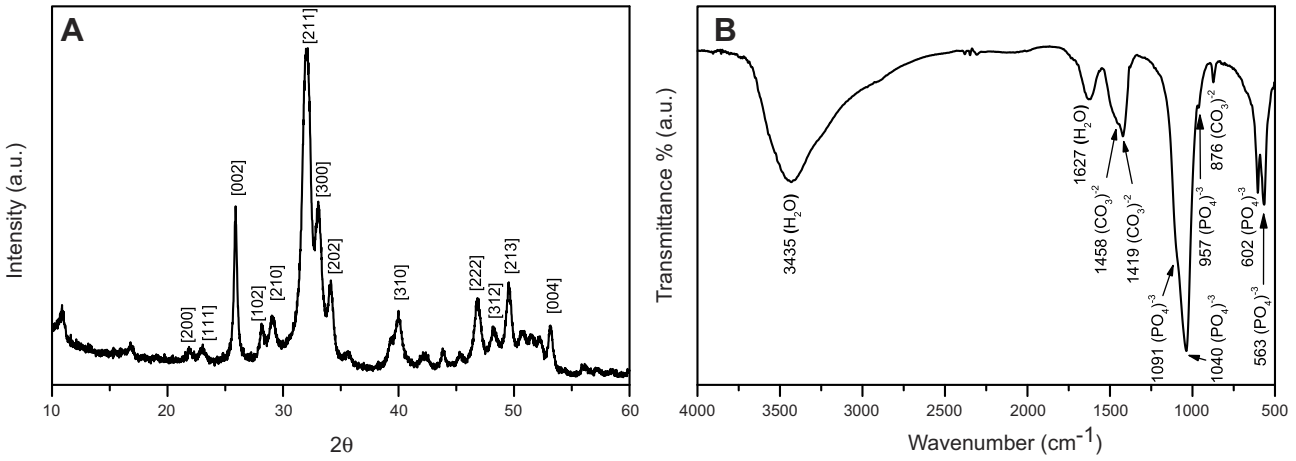

Figure 1 (**A**) X-ray diffractograms and (**B**) infrared spectra of CHA microspheres and minocycline-loaded CHA microspheres.
Abbreviation: CHA, carbonated hydroxyapatite.

Table 1 BET analysis of CHA powder: pore diameter, cumulative pore volume, and cumulative surface area

Pore diameter (nm)	Cumulative pore volume (cm^3)	Cumulative surface area (m^2/g)
94–68	0.116	6.0
68–47	0.241	15.3
47–32	0.356	27.8
32–21	0.441	41.6
21–13	0.505	57.9
13–8	0.542	74.0
8–5	0.558	86.1
5–3	0.561	89.9
3–2	0.566	95.0

Abbreviation: BET, Brunauer, Emmett and Teller Method.

The equivalent CHAMINO mass for inhibiting the bacterial growth was 0.8 mg, 3.1 mg, and 12.5 mg after incubation for 1, 3, and 7 days in the PBS buffer.

Osteoblast cytocompatibility assay

The F-OST osteoblastic cell culture was exposed to a medium containing pure MINO, and to a medium containing CHA and CHAMINO powder extracts and CHA and CHAMINO microspheres, as described in the materials and methods section. As shown in Figure 5, after the cells were exposed to the CHA (powder) extract, the cell viability had a value similar to that of the negative control. Moreover, the CHAMINO (powder) extract exhibited cytotoxicity at the same level of the positive control, which reduced the cell viability by 90%, and at levels similar to those induced by the 0.25% solution of MINO in the F-OST osteoblastic cell culture. However, the cell viability was not affected by the CHA and CHAMINO (microsphere) extracts, which suggests that the alginate somehow protected the fast antibiotic release, and therefore prevented a preliminary drug burst that could impair the viability of the cell.

Histological analysis

Morphological analysis was carried out using a light microscope after the hematoxylin-eosin staining. Figures 6 and 7 show the representative alveolar socket photomicrographs from each implanted biomaterial at 40X magnification. The histological images revealed that the spheres began to degrade during the first implantation period. As shown in Figures 6, 7, and S2, some spheres degraded while others remained intact. After implantation for 42 days, all spheres, CHA, and CHAMINO, were completely degraded. By analyzing the histological images from all implanted periods, we concluded that the CHA and CHAMINO materials exhibited similar degradation behavior. After 7 days, both groups exhibited a mild inflammatory response, which mainly consisted of mononuclear cells, blood vessels of different calibers, and loose connective tissues around the particles, with collagen fibers randomly dispersed in the area. After 7 days, a large area of biomaterial surrounded by connective tissue with abundant hemorrhagic exudate (Figure 6A) was observed in the control group. The CHAMINO group exhibited a few trabeculae of newly formed bone with an osteoblast pavement at the periphery and interspersed by connective tissue containing newformed vessels and fragmented biomaterial (Figure 6B). New bone formation occurred only in contact with the residual bone walls.

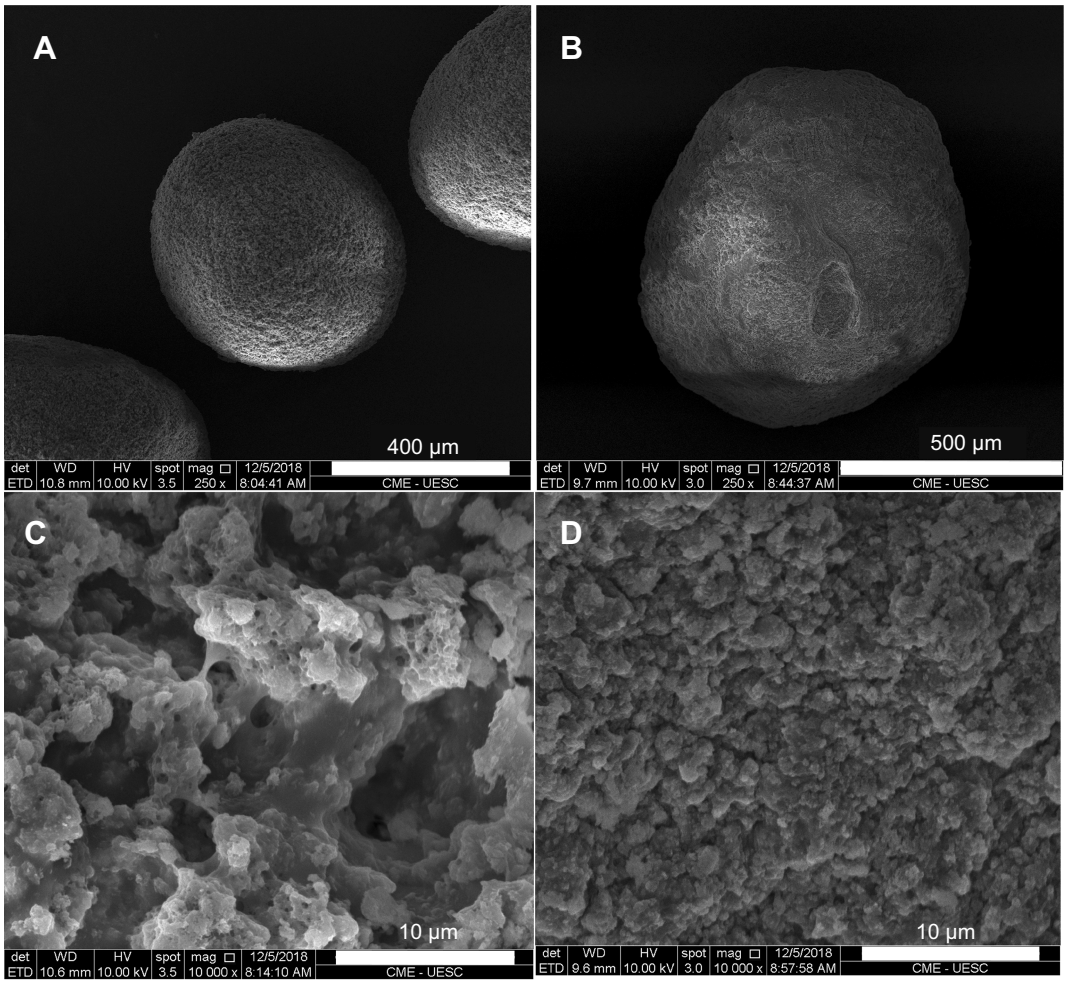

Figure 2 SEM micrographs of cross-section of (**A**) CHA and (**B**) CHAMINO microspheres, and (**C**) surface of CHA and (**D**) CHAMINO microspheres.
Notes: (**A**) and (**B**) magnification =250X (scale bar=400µm); (**C**) and (**D**) magnification=10,000X (scale bar=10µm).
Abbreviations: SEM, Scanning Electron Microscopy; CHA, Carbonated hydroxyapatite; CHAMINO, Minocycline-loaded nanocristalline carbonated hydroxyapatite.

After 42 days, the alveolar socket of both groups was approximately filled by newly formed bone interspersed by connective tissue and remnant hemorrhagic exudate. Inflammatory cells and multinucleated giant cells were rare and localized to the periphery of the CHA and CHAMINO particles, and new bone was observed around the particles (Figure 7A and B). However, most of the particles in the CHA group were surrounded by connective tissue with reduced bone-to-particle contact, which suggests a less robust bone repair process in comparison with the CHAMINO group. At high magnification, it was observed that the trabeculae periphery was surrounded by a large osteoblast pavement. Both biomaterial groups exhibited a reduction in the biomaterial amount compared with the seven-day period. Regions of newly formed bone surrounding the spheres were observed in the CHA group. A reduction in the amount of discernible CHA microspheres was observed between 7 and 42 days. Moreover, it was observed that a considerable amount of newly formed bone surrounded the spheres and the biomaterial particles. Moreover, the final amount of residual graft particles in the CHA group observed after 42 days was similar to that of the CHAMINO group after the same amount of days. In the CHAMINO group (Figure 7B), the newly formed bone appeared to be higher than that in the CHA group (Figure 7A).

Histomorphometric analysis

The bone formation was limited to 7 days after the extraction procedure, and the differences between the CHA and the CHAMINO were not significant (p=0.04). The results obtained by histomorphometric analysis revealed an increase of BV/TV% in both groups between 7 and 42 days after surgery (Figure 8). This indicates a time-dependent increase

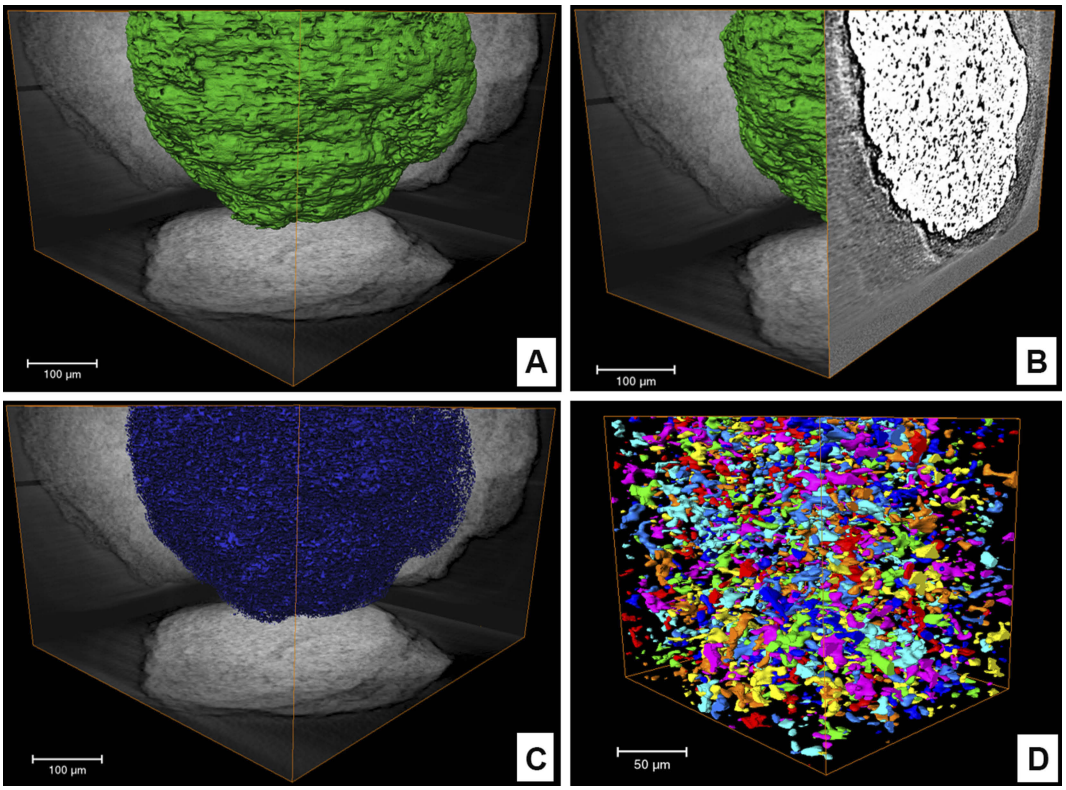

Figure 3 SR-µCT of CHA microsphere: (**A**) VR of microsphere with normalized orthoprojections; (**B**) orthoslice showing porous space inside the sphere; (**C**) VR of porous space inside sphere; (**D**) box representing individual pores of central microsphere region.
Abbreviations: orthoslice, orthogonal slice; SR-µCT, synchrotron radiation-based X ray microtomography; CHA, carbonated hydroxyapatite; VR, volume rendering.

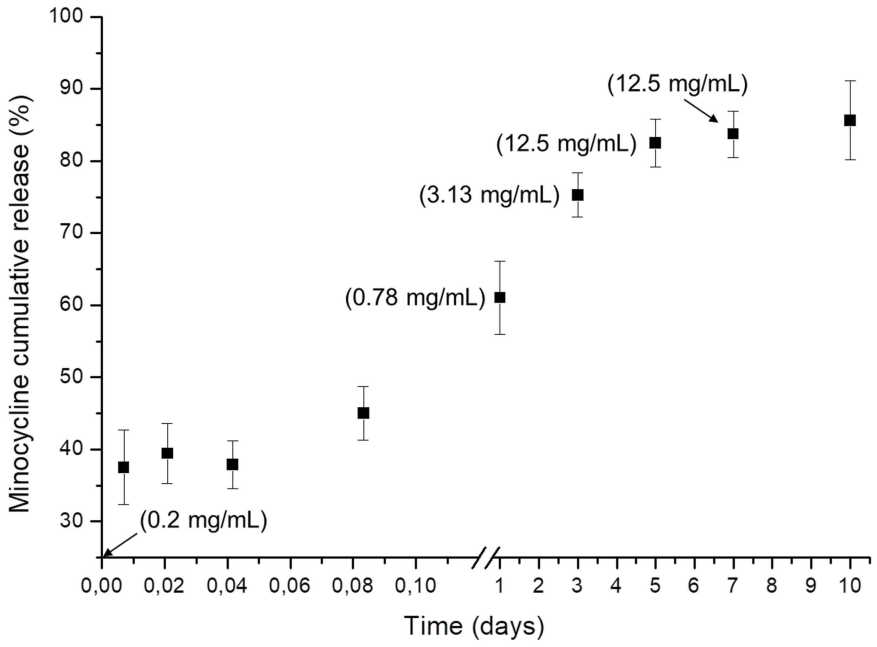

Figure 4 Cumulative MINO (%) release from CHA microspheres in PBS; the MIC values (mg/mL) of the microspheres at 1, 3, 5, and 7 days before and after the MINO release are shown for the *E. faecalis* culture.
Abbreviations: PBS, phosphate-buffered saline solution; MIC, minimum inhibitory concentrations.

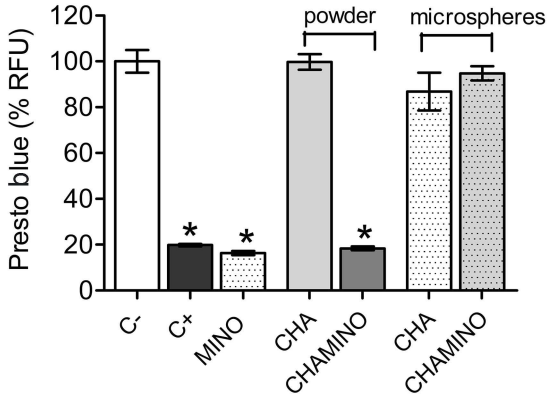

Figure 5 In vitro cell viability using F-OST cells cultured in extracts obtained from CHA and CHAMINO powders and microspheres. Cells seeded over Thermanox coverslip DMEM medium supplemented with 10% FBS were used as the negative control (C-), and 1% sodium dodecyl sulfate (SDS) and MINO 0.25% were used as the positive control, respectively (C+; MINO). Statistical analysis consisted of one-way ANOVA with Dunnett's post hoc test (*p<0.001).
Abbreviations: DMEM, Dulbecco's modified essential medium; FBS, fetal bovine serum; SDS, sodium dodecyl sulfate.

of BV/TV% throughout the experimental period (p<0.05). The bone regeneration underwent a significant (4-fold) enhancement in the CHAMINO group (p=0.001). As expected, both groups exhibited residual particles of grafted material at 7 days after surgery, without significant differences between the groups (p=0.48). A time-dependent biosorption was observed for both groups, as documented by a significant decrease in the BiomatV/TV% of CHA at 42 days after surgery compared with that after 7 days (p<0.01). Similar results were obtained for the CHAMINO group (p<0.01). CHAMINO had significantly more residual BiomatV/TV% at 42 days after healing (p<0.01).

Both groups exhibited varying amounts of connective tissue at 7 days after surgery, and differences were detected between both groups (p=0.10). A time-dependent reduction in the connective tissue volume was observed for the CHAMINO group, as documented by a significant decrease in the CT/TV% at 42 days after surgery compared with that after 7 days (p<0.01). Curiously, the CHA group exhibited increased amounts of connective tissue throughout the experimental period (p<0.01), with significantly more CT volume than CHAMINO after 42 days (p<0.01).

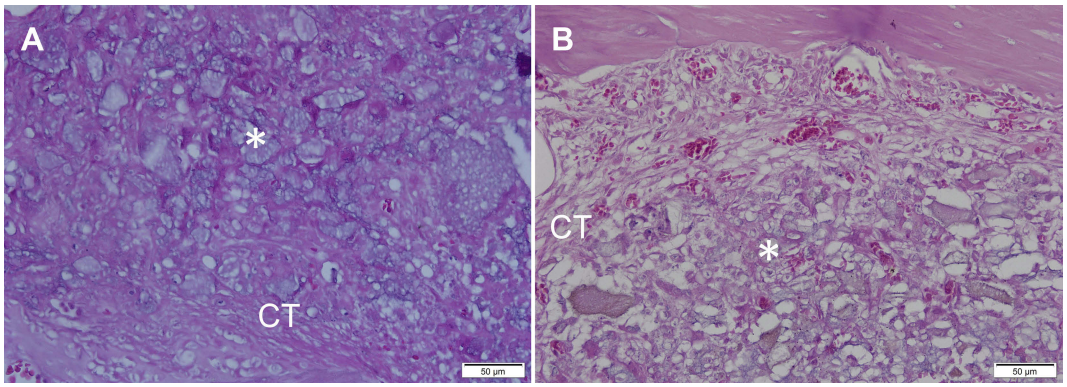

Figure 6 (**A**) One-week CHA and (**B**) CHAMINO groups. After 7 days of implantation, the presence of biomaterial microspheres was observed (**B**) surrounded by connective tissue (CT) and with newly formed bone in the CHAMINO group (*). Magnification: 40X; Stain: Hematoxylin and Eosin.

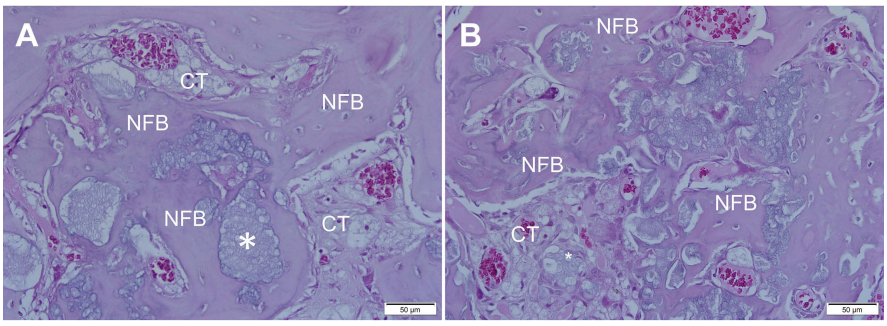

Figure 7 Six-week (**A**) of nanocrystalline carbonated hydroxyapatite (CHA) and (**B**) minocycline-loaded nanocrystalline carbonated hydroxyapatite (CHAMINO) groups. After 42 days of implantation, the residual particles of the biomaterial microspheres were observed surrounded by newly formed bone and connective tissue areas in both groups. Magnification: 40×; Stain: hematoxylin and eosin.
Abbreviations: CT, connective tissue; B, biomaterial; NFB, newly formed bone.

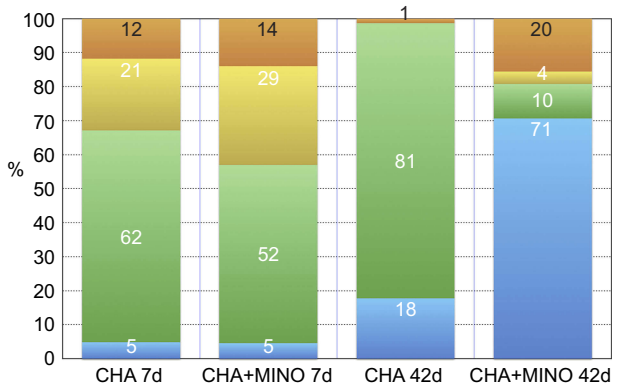

Figure 8 Histomorphometric evaluation of extraction sites following implantation of nanostructured carbonated hydroxyapatite microspheres. Connective tissue (green); biomaterial (yellow); newly formed bone (blue); other (orange).

Discussion

Antibiotics associated with ceramic and non-ceramic hydroxyapatite scaffolds have been proposed for the treatment of infections in bone lesions caused by trauma and degenerative diseases. The advantage of the antibiotic loaded-HA is that it acts simultaneously on the infected defect and the repair of the injured bone. The nanostructured scaffolds allow a more substantial loading of the antibiotic and the faster bioresorption of the biomaterial. However, the remaining challenge can be summarized in three points: the control of antibiotics during the in vivo release, the duration of the bactericidal activity in the injured defect, and the loaded biomaterial toxicity. The scaffold design and its physicochemical characteristics (composition, stoichiometry, microporosity and nanoporosity, and the surface chemical affinity with the antibiotic and bioabsorption) are crucial elements for its biological effects.[3,7]

For the treatment of serious infections, such as osteomyelitis, it is necessary to have a long therapeutic time, and expressive bone repair is needed. Antibiotics belonging to the tetracycline family (tetracycline, doxycycline, and minocycline) have demonstrated a high potential for clinical use when associated with HA.[22] The results obtained by the in vitro experiments revealed that tetracycline-loaded HA/polymer composites increase the proliferation and differentiation osteoblasts and reduce the inflammatory processes.[18] Although several studies have reported that tetracycline acts on the biochemical mechanisms of bone formation, we do not yet have reliable evidence demonstrating the effect of the antibiotic loaded HA on bone regeneration.

This study demonstrated that MINO was successfully adsorbed on nanocrystalline carbonated hydroxyapatite (CHA) powder. The CHA powder had a high specific surface area, which enabled the adsorption of a large amount of MINO per apatite mass (25.1 μg MINO/mg CHA). Despite the weak chemical interaction of the MINO molecule with the CHA surface, the antibiotics were probably trapped by the nanoporosity of the primary agglomerates of the CHA nanoparticles.

Biocompatible CHA microspheres have previously been used as the graft material in bone regenerative therapies, and good results have been obtained.[36–39] These studies have reported that microspheres degrade and are substituted by new bone during the healing stages of the alveolar extraction socket defects in rats. In this study, the microsphere was processed from a mixture of minocycline-loaded CHA powder and soluble biopolymer sodium alginate. The microsphere surface had a smooth roughness that enabled the bone cell attachment. The microsphere interior was composed of CHA NP aggregates bound to the alginate network. BET and μCT analyses revealed that the microsphere had a high specific surface area (72 m^2/g) and microporosity and nanoporosity, which would be entirely available for biological fluids after the alginate dissolution in vivo (Table 1).

The MINO release from the CHA microspheres in the PBS buffer solution had a similar behavior as other antibiotics associated with the hydroxyapatite surface. In the first 24 hrs, 40% of the weakly bond minocycline was released from the large CHA pores. The molecules trapped to very small pores (<94 nm) were probably responsible for the slow release of 60% of the MINO mass that occurred during a period of 10 days. It is worth noting that the release profile of the CHA microsphere was not significantly different to the powder (results are not presented).

The in vitro antimicrobial activity of the CHAMINO microspheres was tested against *E. faecalis*, which is one of the most commonly isolated or detected species in oral infections, including marginal periodontitis, infected root canals, and periradicular abscesses.[40] According to the MIC evaluation, 0.2 mg of CHA loaded with 3 μg of MINO associated with 1 mg of CHA microspheres was necessary to inhibit the growth of *E. faecalis*. The results obtained by the desorption experiments in the PBS buffer revealed that the MINO release from microspheres achieved 75% and 95% of the initial loading mass after 3 and 7 days, respectively. This fast withdrawal from the microsphere led to a 15.5- and 60-fold decrease of the bacterial inhibition (MIC) in 3 days

and 7 days of incubation in the PBS buffer, as shown in Figure 5. These results suggest that the MINO associated with CHA may constitute an antibacterial drug delivery system with a positive potential in treating intra-oral infections.

In vitro and in vivo biocompatibility assays were carried out to estimate the effects of MINO association with CHA on bone regeneration. The data obtained in this study demonstrate that the extracts of CHAMINO did not have negative effects on the osteoblastic cell viability. This conclusion is in accordance with previous studies, which have demonstrated that tetracyclines, and particularly minocycline, do not affect osteoblastic cell survival and proliferation.[17,18,25]

The results obtained by the in vivo evaluation revealed an increase of new bone volume for all experimental periods. Interestingly, the bone regeneration underwent a significant 4-fold enhancement in the CHAMINO microspheres (70.7 versus 17.7%, respectively) after 42 days of healing. This unequivocally demonstrates the positive effects of MINO on the bone regeneration achieved by the CHA biomaterial. To the best of our knowledge, these effects of the locally delivered CHAMINO on bone healing and tissue engineering have not previously been reported. Data on the effects of MINO on bone metabolism and biology in vivo are scarce [41] and demonstrate that the systemic oral administration of the MINO microspheres to ovariectomized rats increases the bone formation-related parameters and reduces the eroded bone surface,[42] which is in accordance with the positive effects documented in this study.

Conclusion

This study demonstrated that alginate encapsulated minocycline-loaded nanocrystalline carbonated hydroxyapatite (CHAMINO) microspheres have an antibacterial activity for *E. faecalis* and exhibit biocompatibility, bioabsorbability, and osteoconduction. These qualities suggest that this material may be promising for targeted antibiotic release in alveolar bone defects during periodontal surgical therapy. Moreover, CHAMINO may enhance the endogenous healing capacity of alveolar bone defects, which significantly improves the bone regeneration modulated by nanocrystalline carbonated hydroxyapatite (CHA). Further investigation is needed to optimize the minocycline delivery rate and understand the role of minocycline in bone regeneration.

Acknowledgments

This study was supported by the Brazilian financial agencies of National Council for Scientific and Technological Development (Conselho Nacional de Desenvolvimento Científico e Tecnológico [CNPq]; grant nos 457541/2013-0 and 467513/2014-7), Foundation for Research Support of the State of Rio de Janeiro (Fundação de Amparo à Pesquisa do Estado do Rio de Janeiro [FAPERJ]; grant nos E-26/102.993/2012 and E-26/203.012/2016), Coordenação de Aperfeiçoamento de Pessoal de Nível Superior-Brasil (CAPES) (Finance Code 001), and National Institute of Science and Technology on Regenerative Medicine (Instituto Nacional de Ciência e Tecnologia em Medicina Regenerativa [INCT Regenera]). The authors wish to thank the IMX beamline of the Brazilian Synchrotron Light Laboratory (LNLS), where the microtomography analyses were performed. We thank Dr Carlos Perez and Helder Valiense from LNLS (XRF Beamline) and Fluminense Federal University (UFF), respectively, for their invaluable contributions to this study.

Disclosure

The authors report no conflicts of interest in this work.

References

1. Dorozhkin SV. Multiphasic calcium orthophosphate (CaPO4) bioceramics and their biomedical applications. *Ceram Int*. 2016;42(6):6529–6554. doi:10.1016/j.ceramint.2016.01.062
2. Habraken W, Habibovic P, Epple M, Bohner M. Calcium phosphates in biomedical applications: materials for the future? *Mater Today*. 2016;19(2):69–87. doi:10.1016/j.mattod.2015.10.008
3. Parent M, Baradari H, Champion E, Damia C, Viana-Trecant M. Design of calcium phosphate ceramics for drug delivery applications in bone diseases: a review of the parameters affecting the loading and release of the therapeutic substance. *J Control Release*. 2017;252:1–17. doi:10.1016/j.jconrel.2017.02.012
4. Kolmas J, Krukowski S, Laskus A, Jurkitewicz M. Synthetic hydroxyapatite in pharmaceutical applications. *Ceram Int*. 2016;42(2):2472–2487. doi:10.1016/j.ceramint.2015.10.048
5. Martin V, Bettencourt A. Bone regeneration: biomaterials as local delivery systems with improved osteoinductive properties. *Mater Sci Eng C*. 2018;82:363–371. doi:10.1016/j.msec.2017.04.038
6. Dorozhkin SV. Calcium orthophosphates (CaPO4): occurrence and properties. *Prog Biomater*. 2016;5(1):9–70. doi:10.1007/s40204-015-0045-z
7. Cazalbou S, Bertrand G, Drouet C. Tetracycline-loaded biomimetic apatite: an adsorption study. *J Phys Chem B*. 2015;119(7):3014–3024. doi:10.1021/jp5116756
8. Kim H-W, Knowles JC, Kim H-E. Porous scaffolds of gelatin-hydroxyapatite nanocomposites obtained by biomimetic approach: characterization and antibiotic drug release. *J Biomed Mater Res Part B Appl Biomater*. 2005;74B(2):686–698. doi:10.1002/jbm.b.30236

9. Guo Y-J, Long T, Chen W, Ning C-Q, Zhu Z-A, Guo Y-P. Bactericidal property and biocompatibility of gentamicin-loaded mesoporous carbonated hydroxyapatite microspheres. *Mater Sci Eng C*. 2013;33(7):3583–3591. doi:10.1016/j.msec.2013.04.021
10. Pourbaghi-Masouleh M, Hesaraki S, Zamanian A, Khanlarkhani A. Gentamicin-PEGylated poor crystalline carbonated hydroxyapatite submicron particles. *Mater Lett*. 2013;113:130–133. doi:10.1016/j.matlet.2013.09.024
11. Parent M, Magnaudeix A, Delebassée S, et al. Hydroxyapatite microporous bioceramics as vancomycin reservoir: antibacterial efficiency and biocompatibility investigation. *J Biomater Appl*. 2016;31(4):488–498. doi:10.1177/0885328216653108
12. Jiang J-L, Li Y-F, Fang T-L, et al. Vancomycin-loaded nano-hydroxyapatite pellets to treat MRSA-induced chronic osteomyelitis with bone defect in rabbits. *Inflamm Res*. 2012;61(3):207–215. doi:10.1007/s00011-011-0402-x
13. Suchý T, Šupová M, Klapková E, et al. The release kinetics, antimicrobial activity and cytocompatibility of differently prepared collagen/hydroxyapatite/vancomycin layers: microstructure vs. nanostructure. *Eur J Pharm Sci*. 2017;100:219–229. doi:10.1016/j.ejps.2017.01.032
14. Šupová M. Substituted hydroxyapatites for biomedical applications: A review. *Ceram Int*. 2015;41(8):9203–9231. doi:10.1016/j.ceramint.2015.03.316
15. Fielding GA, Roy M, Bandyopadhyay A, Bose S. Antibacterial and biological characteristics of silver containing and strontium doped plasma sprayed hydroxyapatite coatings. *Acta Biomater*. 2012;8(8):3144–3152. doi:10.1016/j.actbio.2012.04.004
16. Thian ES, Konishi T, Kawanobe Y, et al. Zinc-substituted hydroxyapatite: a biomaterial with enhanced bioactivity and antibacterial properties. *J Mater Sci Mater Med*. 2013;24(2):437–445. doi:10.1007/s10856-012-4817-x
17. Marycz K, Pazik R, Zawisza K, et al. Multifunctional nanocrystalline calcium phosphates loaded with Tetracycline antibiotic combined with human adipose derived mesenchymal stromal stem cells (hASCs). *Mater Sci Eng C*. 2016;69:17–26. doi:10.1016/j.msec.2016.06.051
18. Gomes PS, Fernandes MH. Effect of therapeutic levels of doxycycline and minocycline in the proliferation and differentiation of human bone marrow osteoblastic cells. *Arch Oral Biol*. 2007;52(3):251–259. doi:10.1016/j.archoralbio.2006.10.005
19. Ratier A, Gibson I, Best S, Freche M, Lacout J, Rodriguez F. Setting characteristics and mechanical behaviour of a calcium phosphate bone cement containing tetracycline. *Biomaterials*. 2001;22(9):897–901.
20. Kaya M, Şimşek-Kaya G, Gürsan N, Kireççi E, Dayı E, Gündoğdu B. Local treatment of chronic osteomyelitis with surgical debridement and tigecycline-impregnated calcium hydroxyapatite: an experimental study. *Oral Surg Oral Med Oral Pathol Oral Radiol*. 2012;113(3):340–347. doi:10.1016/j.tripleo.2011.03.032
21. Čolović B, Pašalić S, Jokanović V. Influence of hydroxyapatite pore geometry on tigecycline release kinetics. *Ceram Int*. 2012;38(8):6181–6189. doi:10.1016/j.ceramint.2012.04.069
22. Pastorino D, Canal C, Ginebra M-P. Drug delivery from injectable calcium phosphate foams by tailoring the macroporosity–drug interaction. *Acta Biomater*. 2015;12:250–259. doi:10.1016/j.actbio.2014.10.031
23. Wang S, Wang X, Xu H, et al. Towards sustained delivery of small molecular drugs using hydroxyapatite microspheres as the vehicle. *Adv Powder Technol*. 2010;21:268–272. doi:10.1016/j.apt.2009.12.001
24. Wang X, Xu H, Zhao Y, et al. Poly(lactide-co-glycolide) encapsulated hydroxyapatite microspheres for sustained release of doxycycline. *Mater Sci Eng B*. 2012;177(4):367–372. doi:10.1016/j.mseb.2011.12.030
25. Trajano VCC, Costa KJR, Lanza CRM, Sinisterra RD, Cortés ME. Osteogenic activity of cyclodextrin-encapsulated doxycycline in a calcium phosphate PCL and PLGA composite. *Mater Sci Eng C*. 2016;64:370–375. doi:10.1016/j.msec.2016.03.103
26. Dou X-C, Zhu X-P, Zhou J, Cai H-Q, Tang J, Li Q-L. Minocycline-released hydroxyapatite–gelatin nanocomposite and its cytocompatibility. *Biomed Mater*. 2011;6(2):025002. doi:10.1088/1748-6041/6/2/025002
27. Ding L, Zhang P, Wang X, et al. Effect of doxycycline-treated hydroxyapatite surface on bone apposition: a histomophometric study in murine maxillae. *Dent Mater J*. 2018;37(1):130–138. doi:10.4012/dmj.2017-007
28. de Souza CAS, Colombo APV, Souto RM, et al. Adsorption of chlorhexidine on synthetic hydroxyapatite and in vitro biological activity. *Colloids Surf B Biointerfaces*. 2011;87(2):310–318. doi:10.1016/J.COLSURFB.2011.05.035
29. Brooks RA, Di Chiro G. Beam hardening in X-ray reconstructive tomography. *Phys Med Biol*. 1976;21(3):004. doi:10.1088/0031-9155/21/3/004
30. Miqueles EX, Helou ES. Fast backprojection operator for synchrotron tomographic data. In: *Progress in Industrial Mathematics at ECMI 2014*. Cham: Springer; 2016:243–252.
31. Koshev N, Helou ES, Miqueles EX. Fast backprojection techniques for high resolution tomography. August 2016:1–32. Available from: http://arxiv.org/abs/1608.03589. Accessed November 12, 2018.
32. Kornman KS, Robertson PB. Clinical and microbiological evaluation of therapy for juvenile periodontitis. *J Periodontol*. 1985;56(8):443–446. doi:10.1902/jop.1985.56.8.443
33. Balduino A, Hurtado SP, Frazão P, et al. Bone marrow subendosteal microenvironment harbours functionally distinct haemosupportive stromal cell populations. *Cell Tissue Res*. 2005;319(2):255–266. doi:10.1007/s00441-004-1006-3
34. ISO 10993-5:2009(en). Biological evaluation of medical devices — part 5: tests for in vitro cytotoxicity. Available from: https://www.iso.org/obp/ui/#iso:std:iso:10993:-5:ed-3:v1:en. Accessed November 28, 2018.
35. Kilkenny C, Browne W, Cuthill IC, Emerson M, Altman DG. Animal research: reporting in vivo experiments: the ARRIVE guidelines. *Br J Pharmacol*. 2010;160(7):1577–1579. doi:10.1111/j.1476-5381.2010.00872.x
36. Soriano-Souza CA, Rossi AL, Mavropoulos E, et al. Chlorhexidine-loaded hydroxyapatite microspheres as an antimicrobial delivery system and its effect on in vivo osteo-conductive properties. *J Mater Sci Mater Med*. 2015;26(4):166. doi:10.1007/s10856-015-5505-4
37. Calasans-Maia MD. de Melo BR , Alves ATNN, et al. Cytocompatibility and biocompatibility of nanostructured carbonated hydroxyapatite spheres for bone repair. *J Appl Oral Sci*. 2015;23(6):599–608. doi:10.1590/1678-775720150122
38. Machado CPG, Sartoretto SC, Alves ATNN, et al. Histomorphometric evaluation of strontium-containing nanostructured hydroxyapatite as bone substitute in sheep. *Braz Oral Res*. 2016;30:1. doi:10.1590/1807-3107BOR-2016.vol30.0045
39. Da Suruagy AAPS, Alves ATNN, Sartoretto SC, de Calasans-Maia JA, Granjeiro JM, Calasans-Maia MD. Physico-chemical and histomorphometric evaluation of zinc-containing hydroxyapatite in rabbits calvaria. *Braz Dent J*. 2016;27(6):717–726. doi:10.1590/0103-6440201601028
40. Kayaoglu G, Ørstavik D. V irulence F actors of *E nterococcus faecalis*: R elationship to E ndodontic D isease. *Crit Rev Oral Biol Med*. 2004;15(5):308–320.
41. Williams S, Wakisaka A, Zeng QQ, et al. Minocycline prevents the decrease in bone mineral density and trabecular bone in ovariectomized aged rats. *Bone*. 1996;19(6):637–644.
42. Williams RC, Paquette DW, Offenbacher S, et al. Treatment of periodontitis by local administration of minocycline microspheres: a controlled trial. *J Periodontol*. 2001;72(11):1535–1544. doi:10.1902/jop.2001.72.11.1535

Supplementary materials

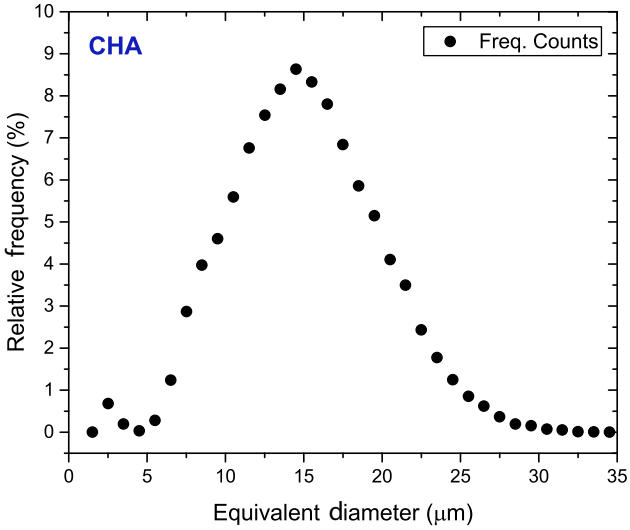

Figure S1 Equivalent pore diameter distribution of nanocrystalline carbonated hydroxyapatite (CHA) microsphere determined by SR-μCT.
Abbreviations: SR-μCT, synchrotron radiation-based X ray microtomography.

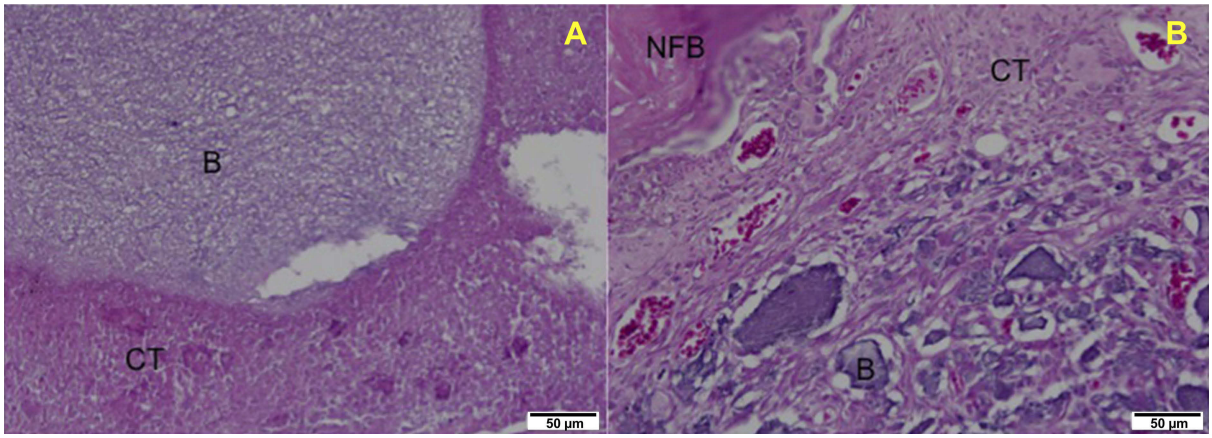

Figure S2 (**A**) One-week nanocrystalline carbonated hydroxyapatite (CHA) and (**B**) minocycline-loaded nanocristalline carbonated hydroxyapatite (CHAMINO) groups. After one week of implantation, the presence of non-degraded CHA microspheres was observed surrounded by connective tissue and with newly formed bone in the CHAMINO group. Magnification: 40×; stain: Hematoxylin and Eosin.
Abbreviations: B, biomaterial; NFB, newly formed bone; CT, connective tissue.